Three-dimensional boundary layer transition on a concave surface

G. Leoutsakos and R. I. Crane
Department of Mechanical Engineering, Imperial College of Science, Technology & Medicine, Exhibition Road, London SW7 2BX, UK

Measurements of streamwise mean and r.m.s. velocity, intermittency factor and energy spectra are reported for a laminar boundary layer undergoing transition on a concave wall in the presence of a naturally occurring Görtler vortex system, concentrating on a particular vortex pair. The ratio of boundary layer thickness to wall radius at the start of curvature was 0.01. Nonlinear amplification of the vortices, followed by spanwise meandering and a secondary instability, preceded transition, which was defined in terms of the intermittency factor after filtering out low frequencies associated with this vortex behavior. Transition was initiated in the vortex upwash region and apparently completed within a streamwise distance of only a few boundary layer thicknesses at both upwash and downwash locations, implying rapid lateral spreading of turbulence. With considerable velocity profile distortion prior to transition, values of momentum thickness Reynolds number and Görtler number at start of transition, either upwash-localized or upwash-downwash averaged, did not correspond well with established correlations for flat surfaces or with earlier concave-wall studies.

Keywords: boundary layers; transition; Görtler vortices; longitudinal curvature

Introduction

The operational characteristics and the efficiency of turbomachines are strongly influenced by the behavior of the boundary layers developing on the blading surfaces. In the case of gas turbines, operating at turbine inlet gas temperatures substantially above the structural limits of the high-temperature alloys used for the components, blade boundary layer flow and convective heat transfer predictions are of great importance at the design stage, principally in order to minimize the requirements for blade cooling air but also to optimize blade aerodynamic efficiency. A particular area of interest is the blade pressure surface, where considerable uncertainty can exist over the boundary layer state at a particular streamwise location. This uncertainty is expected in a boundary layer containing laminar, transitional, and turbulent regions, subjected to the destabilizing effects of concave curvature and turbulent energy entrainment from the free stream and the stabilizing influence of a favorable pressure gradient, with the possibility of a three-dimensional (3-D) Görtler vortex structure.

Pressure–surface boundary layers that possess 3-D characteristics are unlikely to be predicted accurately by the two-dimensional (2-D) codes in current use. The deficiencies exist mainly in the modeling of laminar–turbulent transition, which is done explicitly in the earlier (and still commonly used) codes by empirical correlations (see, e.g., Ref. 1), to fix the start and length of transition. The more recent and generally more successful prediction codes employ low Reynolds number, higher order turbulence modeling (see, e.g., Ref. 2) to compute automatically through transition. Poor agreement has often been found between predictions and experimental data for blade pressure surfaces, as demonstrated for instance by Daniels and Browne[1] who compared cascade measurements with numerical predictions from five different models. Further work is needed to attain a greater understanding of the process and characteristics of transition on concave surfaces and hence "tune" the prediction models in order to obtain higher reliability and accuracy.

Transition may sometimes be initiated via a separation bubble near the leading edge; most prediction methods would be unable to compute through laminar separation with turbulent reattachment. Furthermore, blade rotation, compressibility, vibration, surface roughness variation, etc., make the behavior of the boundary layer even harder to predict. However, it is widely believed that Görtler vortices are involved to some extent in natural transition on concave surfaces and that their development and breakdown should be the subject of further research. Such flow structures have been observed[3] on blade pressure surfaces in cascade experiments. Conditions in gas turbine engines are appropriate for their occurrence, and they may play a major role in the transition process as well as possibly increasing laminar heat transfer rates.

The purpose of the present work is to provide experimental information on the fundamental processes involved in the breakdown of adiabatic laminar flow on a concave wall and to identify the characteristics of transition through successive stages of vortex nonlinear development and unsteadiness. It is hoped that the results, together with those of similar work elsewhere (see, e.g., Ref. 4), will assist in the development of improved spanwise-averaged transition criteria, and hence provide a short-term means to more reliable blade heat transfer predictions via existing codes of the 2-D parabolic finite-difference type (with low-order turbulence models). Such prediction codes, e.g., GENMIX in Ref. 5, still stand as good a chance of producing usable predictions, e.g., Ref. 6, as higher order and more elaborate codes, e.g., that in Ref. 7, and have the advantage of being fast and cheap to run.

This paper describes adiabatic flow experiments on a constant-curvature wall at momentum thickness Reynolds numbers and Görtler numbers not too different from those expected under gas turbine working environments. It complements the measure-

Address reprint requests to Dr. Crane at the Department of Mechanical Engineering, Imperial College of Science, Technology and Medicine, Exhibition Road, London SW7 2BX, UK.

Received 13 March 1989; accepted 8 July 1989

ments presented in Ref. 8 and includes flow visualization, streamwise and spanwise variations of mean and r.m.s. streamwise velocity, measurements of the intermittency factor, and energy spectra before and during transition. The tests were carried out mainly within a particular Görtler vortex pair.

Empirical prediction of transition

A great deal of theoretical and experimental work has been done on the instability of laminar boundary layers and in determining criteria for modeling transition, which is characterized by the intermittent appearance of turbulent spots moving downstream with the fluid, with laminar flow in their trail. Turbomachinery blading predictions have frequently ignored the transition region and considered a step change from laminar to turbulent flow, an assumption that produced inaccurate assessments of boundary layer behavior owing to the relatively large extent of the transition region. Empirical transition modeling consists of identifying the start and end (or length) of transition and also the variation of flow properties within that interval, commonly determined by the variation of the intermittency factor γ defined for any point in the flow as the fraction of total time that the flow is turbulent. Several correlations exist for the start of transition on a flat surface. Most of them are in terms of the momentum thickness Reynolds number $\mathrm{Re}_{\theta S}$ at transition start, as for instance that by Abu-Ghannam and Shaw[9]:

$$\mathrm{Re}_{\theta S} = 163 + \exp\left(F(\Lambda_\theta) - \frac{F(\Lambda_\theta)}{6.91}\, Tu\right) \tag{1}$$

where $F(\Lambda_\theta)$ is a function of the pressure gradient parameter $\Lambda_\theta = (\theta^2/\nu)(du_e/dx)$ and Tu is the free-stream turbulence level (expressed as a percentage); θ is the momentum thickness, ν the kinematic viscosity, u_e the boundary layer edge velocity and x the streamwise coordinate. Similar formulas for the transition onset point are given in Refs. 10–12, etc., and are in broad agreement for flat plate transition for zero and adverse pressure gradients, whereas for favorable pressure gradients some investigators, as in Ref. 9, predict a more rapid increase of $\mathrm{Re}_{\theta S}$ with increasing Λ_θ and Tu than others. Similar work has also been published for estimating the transition length (or end point), as for instance in Ref. 9:

$$\mathrm{Re}_{\theta E} = 540 + 183.5(\mathrm{Re}_L \times 10^{-5} - 1.5)(1 - 1.4\Lambda_\theta) \tag{2}$$

where Re_L is the Reynolds number based on the transition length L, or the work by Dhawan and Narasimha,[13] who produced a similar relation linking $\mathrm{Re}_{\theta E}$ to $\mathrm{Re}_{\theta S}$. These authors also gave a popular description of the variational form of intermittency within the transition region, namely,

$$\gamma = 1 - \exp(-A\xi^2) \tag{3}$$

where A is a constant and ξ a normalized streamwise coordinate in the transition zone. Other types of functional distributions for γ (mainly exponential) can be found in Refs. 14, 15, etc. Introducing curvature adds the complication of a centrifugal force acting on the flow. Comparatively little is known about the effects of curvature on transition, although a number of investigations have been made on the topic from as early as 1943 by Liepmann[16] until the present time (see, e.g., Refs. 4 and 17). The earlier data were combined with other factors affecting transition in the model of Forest,[6] which included the Görtler number G_θ in the modeling equations and took into account the effects of curvature, pressure gradient, and free-stream turbulence through semi-empirical equations including the modification of the turbulent mixing length l_c. He considered transition to be the outcome of the combination of two different types of instability: the Tollmien–Schlichting type and the Görtler type. The resulting correlations, used by a number of gas turbine manufacturers, appear to produce acceptable predictions on blade suction surfaces but not on pressure surfaces, seemingly the weak point of all prediction methods. Broad agreement exists in the treatment of the mixing length under the effects of curvature, as in, e.g., Refs. 18 and 19. Work has also been reported of curvature effects on thermal diffusivity.[20] Transition suppression or flow relaminarization should also be considered for accelerating flows such as on the surfaces of prescribed-velocity-distribution blades. The Jones and Launder[21] relaminarization criterion, i.e., K (velocity gradient parameter $= (\nu/u_e^2)\, du/d$) greater than 2.5×10^{-6}, is in common use. Brown and Martin[22] suggested that the same criterion be applied to design for the prevention of transition.

Assessment of the flow properties of a transition region by methods such as those in Refs. 6 and 23 requires knowledge of the state and characteristics of the laminar and turbulent counterparts that comprise it. Once they are known they can be linked by weighting them by means of an equation of the form

$$D_{\mathrm{eff}} = D_l + \gamma D_t \tag{4}$$

Notation

- A Amplitude of $\bar{u}(z)$ distribution
- a Test section width (in radial direction)
- D Diffusivity
- G_θ Görtler number, $\mathrm{Re}_\theta(\theta/R)^{1/2}$
- K Velocity gradient parameter, $(\nu/u_e^2)\, du_e/dx$
- R Outer wall radius of curvature
- Re Reynolds number
- Tu Turbulence intensity $\tilde{u}/\bar{u}$
- u Streamwise velocity component
- x Streamwise coordinate
- y Coordinate normal to concave wall
- z Spanwise coordinate

Greek letters

- α Wavenumber $2\pi/\lambda$
- γ Intermittency factor
- δ Boundary layer physical thickness
- θ Boundary layer momentum thickness
- Λ_θ Velocity gradient parameter $(\theta^2/\nu)\, du_e/dx$
- λ Görtler vortex wavelength
- ν Kinematic viscosity
- φ Angular coordinate x/R

Subscripts

- a Based on test section width a
- E At end of transition
- e At boundary layer edge (flat wall)
- L Based on length of transition zone
- l In laminar flow
- pw Wall value in potential flow
- S At start of transition
- t In turbulent flow
- x Based on streamwise distance

Superscripts

- $\bar{}$ Time-mean value
- $\tilde{}$ R.m.s. value of fluctuating quantity

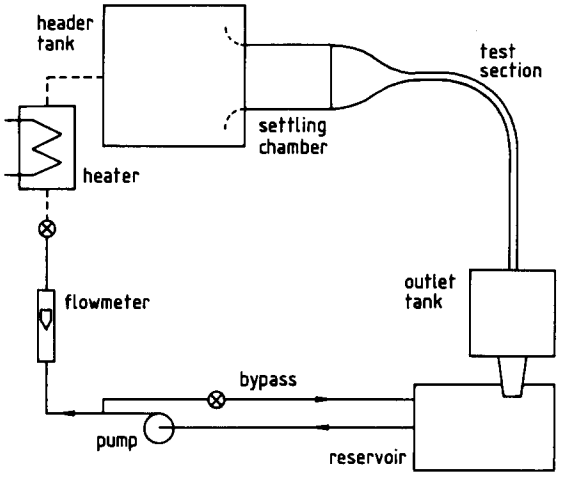

Figure 1 Diagram of flow circuit

where γ varies from 0 to 1, gradually switching on the turbulent diffusivity D_t and adding it to the laminar diffusivity D_l.

To improve confidence in finite-difference codes incorporating such transition region predictions (pending the further development and acceptance of higher order models that compute automatically the transition region development), more experimental evidence is needed to support the models and establish reliable values for important thresholds that are necessary in order for the codes to run. This is especially true in the case of curved surfaces.

Experimental arrangement

Flow rig

The flow rig used was of the closed circuit type, shown schematically in Figure 1. Water was chosen as the working fluid to simplify flow visualization and laser-Doppler velocity measurement. The flow was gravity driven, with a constant-speed radial pump serving to transfer water from the reservoir tank to the header tank. Some 13 m of piping (indicated by the dashed line in Figure 1) were inserted upstream of the header tank to damp out any vibrations or pressure waves coming from the pump that could affect the hot-film anemometer readings by introducing unwanted frequencies. A 5 kW heater was incorporated in the system to help maintain a constant water temperature. The flow was monitored using a cone-and-float flowmeter. The settling chamber, fed from the header tank, contained a bank of glass balls (24 mm diameter), perforated plates and four brass woven screens of 1 mm mesh size. Figure 2 illustrates the 90° constant-cross-section bend, with outer wall radius $R = 500$ mm; it was preceded by a 9:1 area ratio, concave–convex wall contraction and followed by a length of straight duct. The aspect ratio was 6:1. This arrangement provided a suitable Görtler vortex configuration, repeatable from run to run.

Instrumentation

A laser-Doppler anemometer (LDA) was used for mean and r.m.s. velocity measurements and a constant temperature hot-film anemometer (CTA) for detection of the start and end of transition and evaluation of the intermittency factor γ. The CTA was preferred to the LDA for the intermittency factor because of the large signal dropout from the LDA, compared to the CTA's continuous signal. Only the streamwise component of velocity was measured, mean and r.m.s. values being denoted by $\bar{u}$ and $\tilde{u}$ respectively. The LDA system was operated in the forward-scatter fringe mode using a 5 mW He–Ne laser. Signals were processed by using a Cambridge Consultants CC08 frequency-tracking demodulator. The maximum uncertainties in $\bar{u}$ and $\tilde{u}$ were estimated as $\pm 3\%$ and $\pm 4\%$, respectively. The CTA probe was a Dantec 55R15 boundary layer fibre-film probe, powered by a Dantec 56C CTA system. Its active length was 1.25 mm, the operating temperature 120°C, and the overheat ratio 1.3. The quartz-coated waterproof probe was mounted on a traversing mechanism providing one translational movement in the spanwise (vertical) direction z and rotation about a z-axis offset in the streamwise (x) direction from the probe head, allowing measurements to be taken along an arc approximating the y-direction (normal to the curved walls). The probe was inserted into the test section through one of a set of holes on the top end wall of the channel (shown in Figure 2), depending on the streamwise location where measurements were to be taken. The correct positioning of the probe was occasionally checked by focusing the laser beam intersection, whose precise location was known, on the sensor element of the film probe. A more detailed description of the LDA and CTA systems is given in Refs. 8 and 14.

The data acquisition system for both the LDA and CTA consisted of a Tecmar AD211 12-bit analogue-to-digital converter and Apple IIe microcomputers (one for each system). The stored data, sampled at 4 kHz, was processed using purpose-written assembly language programs. For the CTA system the input to the A/D converter was conditioned through a dual (high and low pass) filter and a precision gain-and-offset amplifier. The software processed eight batches of 17,000 samples each, giving the mean and r.m.s. velocities and intermittency factor values in less than one minute. Filter settings, critical to the results, were selected after an extensive investigation of the flow frequencies using a spectrum analyser. This involved consideration of: (a) the value of U/δ (U = core flow velocity, δ = boundary layer thickness) indicating the frequency of the largest eddies; (b) the values of preferred frequencies in the flow during the later, unsteady stages of Görtler vortex development; (c) values of unwanted frequencies that had to be excluded, such as the pump impeller blade passing frequency; (d) electronic noise of the order of kHz. High-pass filter settings varied from 36 Hz to 8 Hz as the probe location moved downstream and δ increased. Low-pass filtering was set at 60 Hz for locations prior to the middle of the bend ($\varphi = 45°$; angle φ is defined in Figure 2) and then increased (through 100 Hz at $\varphi = 60°$) until the bend exit. Extensive testing of the software for intermittency evaluation (using electronically simulated turbulence signals and a flat-plate boundary layer flow) indicated that any measured value of γ exceeding 90% should be taken

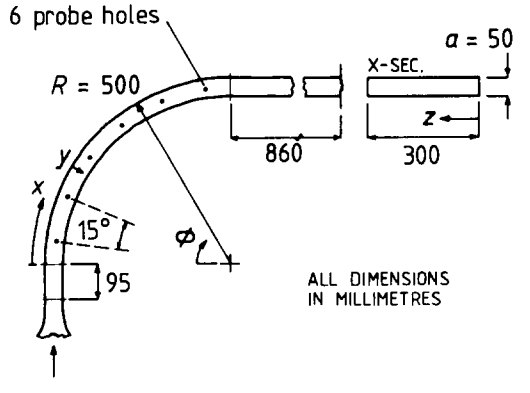

Figure 2 Detail of test section (all dimensions in mm)

to represent fully turbulent flow. Online plotting was provided by an Acorn BBC-B microcomputer coupled serially to the Apple (because of its superior graphics facilities), building up mean and r.m.s. velocity profiles as the experiments were being carried out. Energy spectra of the flow fluctuations were obtained through the CTA system by feeding the unprocessed hot-film probe output to a spectrum analyser (Spectra Dynamics). More details of the instrumentation have been given in Refs. 8 and 14. Flow visualization was carried out using the hydrogen-bubble technique, proving invaluable in identifying the location and shape of vortex pairs and indicating the most appropriate streamwise and spanwise positions for LDA and film-probe traversing. By switching the current through the cathode wire (25 μm diameter) successive rows of bubbles (*time lines*) were generated to give an indication of the spanwise distributions of mean velocity. Continuous sheets of bubbles were more useful in revealing vortex growth and breakdown.

Experimental procedure and flow conditions

The flow rate was set at 190 l/min, corresponding to Re_a (based on a channel width of $a=50$ mm) of 10,500; this rate gave an initially laminar boundary layer which became fully turbulent (in the sense of near-unity intermittency factor at all spanwise locations within the chosen vortex pair) and also ceased to exhibit spanwise variation of mean velocity before the bend exit. Measurements were obtained at two spanwise (z) positions, approximately 185 and 192 mm from the channel bottom, corresponding to the regions of upwash, where low momentum fluid is swept away from the wall, and downwash, where core-flow fluid moves toward the wall. The spanwise positions of these two regions varied slightly (1–2 mm) between streamwise stations. This particular vortex pair was chosen because it appeared to exhibit secondary instability at an earlier streamwise position than any other pair. Transition at other spanwise positions was expected to be influenced by lateral spread of turbulence from adjacent regions where vortices had undergone earlier breakdown. The chosen position was also close enough to the upper end wall to avoid serious flow-induced vibration of the hot-film probe stem, while not being significantly affected by end-wall secondary flow.

The LDA and CTA measurements were made at 11 streamwise stations, at distance intervals selected to ensure an adequate number of measurements within the transition region. The streamwise pressure gradient was small and slightly favorable ($K<0.12\times10^{-6}$); the streamwise variation of potential wall velocity u_{pw} is plotted in Figure 3. The turbulence intensity in the pseudo-potential core flow was in the range of 2–3%. Traverses in the y-direction were made in 2-mm steps within the boundary layer and in 4-mm steps outside. Although the LDA and CTA traverses were carried out separately, frequency analysis and intermittency measurements were taken simultaneously, recording spectral plots at every location where γ was evaluated.

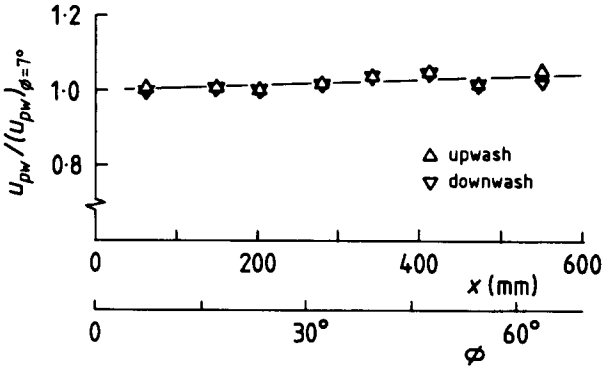

Figure 3 Streamwise variation of potential wall velocity u_{pw} (normalized by value at $\varphi=7°$)

Results

From the mean velocity profiles in Figure 4(a), differences between the regions of upwash and downwash become apparent at $\varphi=17°$, the vortices developing further with increasing streamwise distance and growing into the core flow. Vortex wavelength λ and spanwise position remained virtually unaltered through the bend. Boundary layer thickness δ varied from 5 mm ($\delta/R=0.01$) at $\varphi=7°$ to 25 mm ($\delta/R=0.05$) at $\varphi=83°$. Except in these early and late stages of vortex development, large spanwise variation was observed in boundary layer parameters (δ, displacement thickness δ^*, θ) between upwash and downwash.

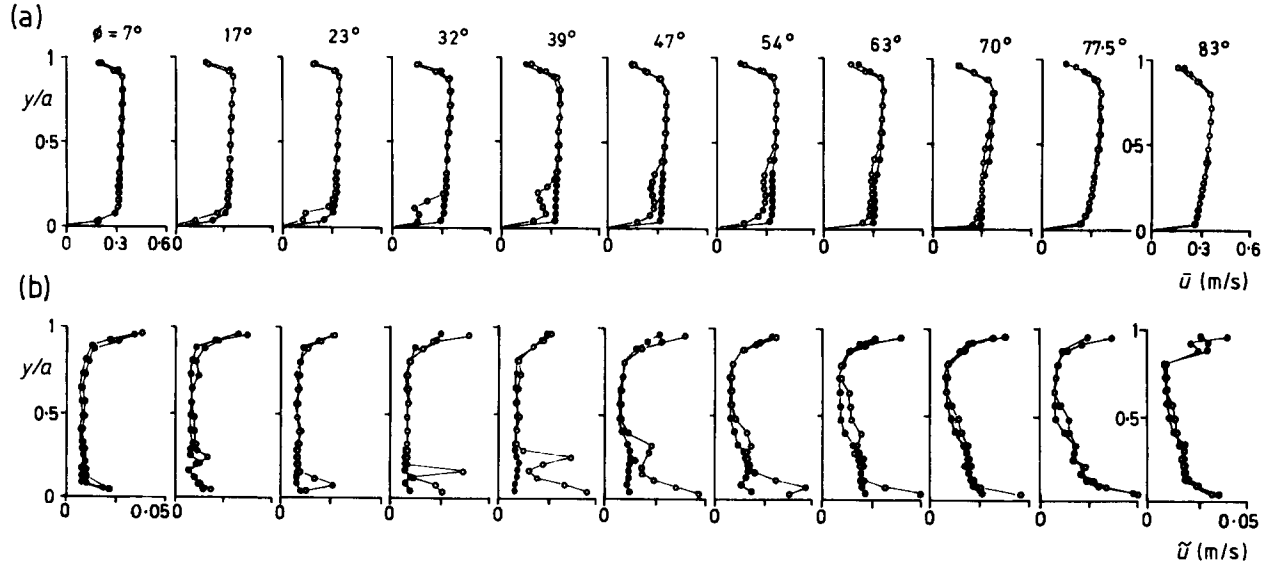

Figure 4 Streamwise development of profiles of (a) mean velocity $\bar{u}$ and (b) r.m.s. fluctuating velocity $\tilde{u}$, at $Re_a=10{,}500$

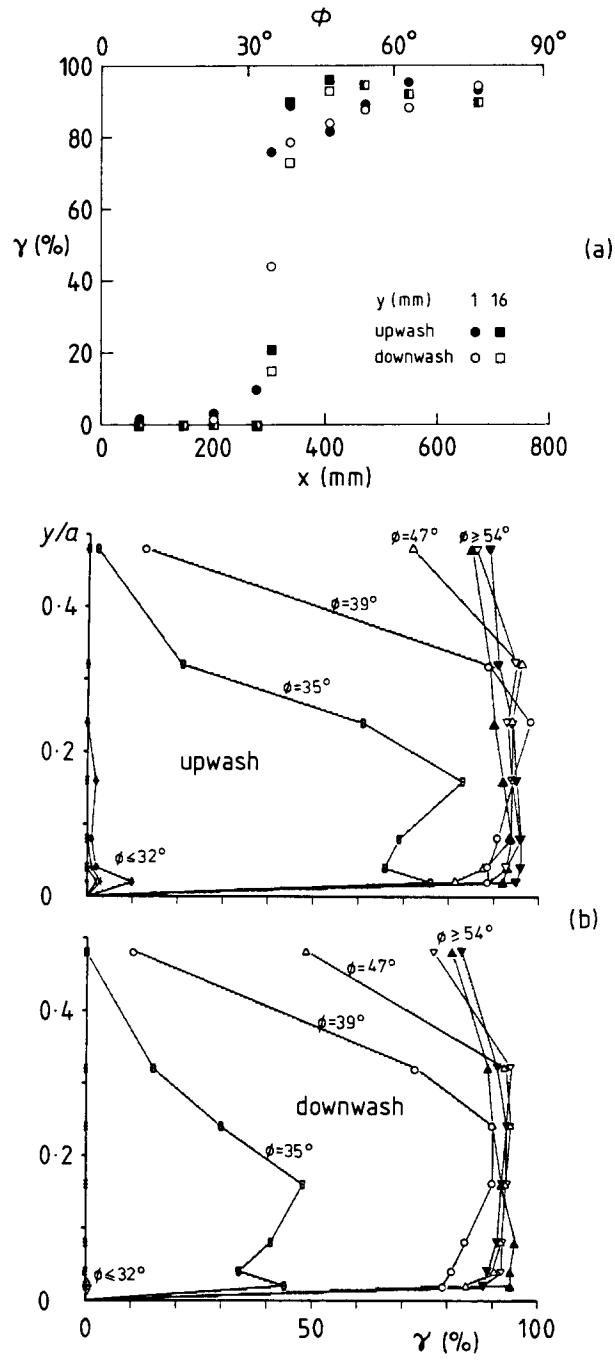

Figure 5 (a) Streamwise and (b) normal variation of intermittency factor γ, at $Re_s = 10{,}500$

The variation of intermittency factor with streamwise distance [Figure 5(a)] indicates transition starting near $\varphi = 32°$ and finishing by $\varphi = 39°$, implying a very short transition length (typically 4δ at upwash). The profiles of intermittency [Figure 5(b)] show 0 or very low γ values over the whole of the boundary layer (in the y–z plane), abruptly increasing to fully turbulent values ($\gamma > 90\%$), again for the whole of the boundary layer, within the short transition interval. The intermediate stage at $\varphi = 35°$, where γ (spanwise averaged) is approximately 0.5, is the only location where two local maxima are observed in the γ *versus* y curves, one near the wall and another in the high-shear region away from the wall. Fluctuating velocity ($\tilde{u}$) profiles [Figure 4(b)] also show a second local maximum attaining its highest value at $\varphi = 39°$. The two local maxima, which may both mark sites for breakdown of the flow and generation of turbulence, are slowly smoothed out because of diffusion on moving downstream.

Streamwise variation of integral boundary layer parameters is shown in Figure 6. The momentum thickness Reynolds number Re_θ is approximately equal to 120, and the Görtler number G_θ is equal to 3 at $\varphi = 7°$, with little difference between upwash and downwash. Before and during transition, Re_θ and G_θ at upwash increased monotonically with streamwise distance, reaching 500 and 30, respectively, at the measured transition start position, then approaching 650 and 45, respectively, at transition end with a reduced rate of increase. Values at downwash remained below $Re_\theta = 100$ and $G_\theta = 4$. Following the end of transition, the upwash and upwash–downwash averaged values of Re_θ and G_θ decreased, approaching their bend-entry values near the bend exit, where the intermittency was everywhere near unity and the spanwise variation in velocity almost vanished. For $\varphi > 80°$, Re_θ appears to be very low for sustaining a turbulent boundary layer, but it may be influenced by the favorable pressure gradient as the end of curvature is approached. Upwash–downwash averaged Re_θ at transition start was approximately 260 ($\theta/R \approx 0.0025$) compared with $Re_\theta \approx 190$ calculated for the same streamwise station on a flat plate (effective boundary layer origin based on the measured boundary layer thickness at $\varphi = 7°$). Flat-plate transition would be expected (see Ref. 9) to start at $Re_\theta \approx 200$ for the present 3% core-flow turbulence intensity. Based on the single vortex pair

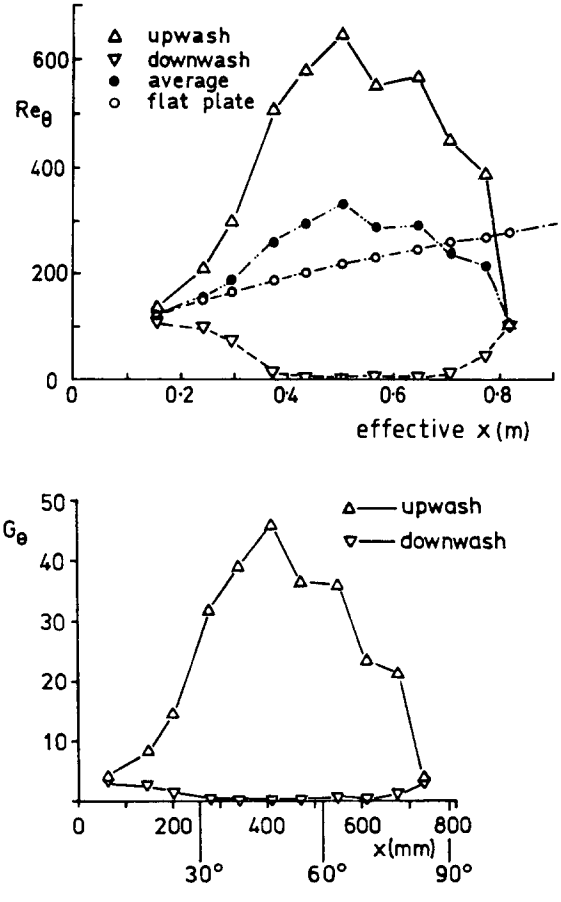

Figure 6 Streamwise variation of momentum thickness Reynolds number Re_θ and Görtler number G_θ

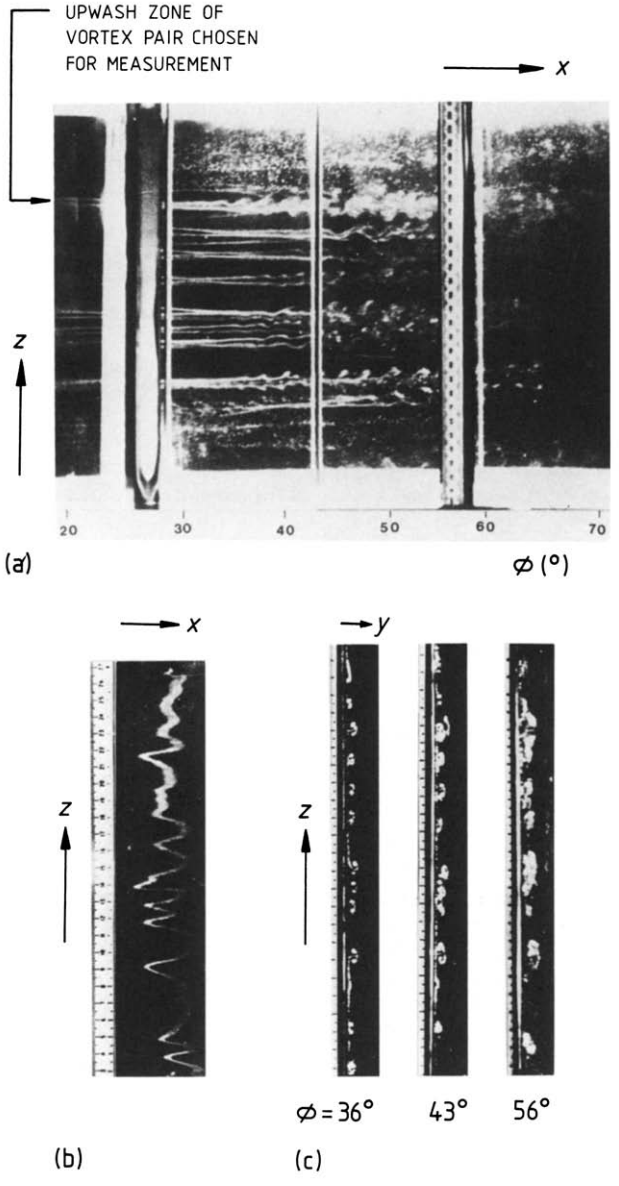

Figure 7 Hydrogen-bubble visualization of Görtler vortex development at $Re_\delta = 10{,}500$: (a) approximately radial view of whole test section; (b) time line near $\varphi = 20°$; and (c) streamwise view of cross sections

measured, it appears that the effect of the vortex system (and other influences of curvature) was to increase the boundary layer growth rate such as to delay transition in terms of Re_θ but not in terms of Re_x. This effect contrasts with earlier measurements (see Ref. 8) on a higher curvature surface, where upwash-localized Re_θ at transition start was reasonably close to the flat-plate transition-onset value. However, neither the present data nor those in Ref. 8 are directly comparable with the more comprehensive data presented in Ref. 17, for which θ/R values were much smaller than ours and where velocity profiles did not suffer the same degree of distortion. In the present flow, the upwash–downwash averaged Re_θ is not representative of a spanwise average because downwash regions occupy a greater fraction of the span than do upwash regions following distortion of the vortices.

Photographs of hydrogen bubbles showing streak lines, time lines, and cross-sectional patterns of the flow are presented in Figure 7. The streak lines show that vortex pairs at different stages of development coexist at the same streamwise location; time lines and cross-sectional views also indicate that neighboring vortex pairs can possess widely differing strength and size.

After the initial formation of the vortices in the early part of the bend, their development until they reach a turbulent state may be divided into four stages. During the first stage, here called linear because of the correspondence with the idealized vortex structure described by mathematically linear equations, the vortices approximate pairs of longitudinal rotating cylinders with circular cross sections. These become elliptical and sometimes skewed in the second, nonlinear stage. Vortex strength is continuously intensified by the energy supply from the mean velocity and centrifugal force fields. The third stage, the transitional region, follows next, appearing to occupy the region from $\varphi = 32°$ to $\varphi = 39°$. When different filtering is used on the anemometer signal so as to alter the effective definition of intermittency and count only the "conventional" turbulent spots, excluding the low-end preferred frequencies, the apparent transition region shifts downstream to between $\varphi = 40°$ and $\varphi = 47°$, the transition length remaining approximately constant. Transition manifests itself first by a meandering motion of the vortices, here oscillating at approximately 16 Hz. Bippes and Görtler [25] and others have also reported meandering motion in the early stages of transition. With meandering still present, another form of secondary instability occurs 3°–5° (approximately 2δ) farther downstream in the form of a pulsating 3-D vortex, consistent with a horseshoe-type vortex detected by Aihara and Koyama.[26] Although this secondary instability has been associated with the high-shear zone in the upwash $\bar{u}$ *versus* y profile, inflections in the $\bar{u}$ *versus* z distribution have recently[27] been suspected to play a more important role. As this vortex breaks up, "pulsing" at around 28 Hz produces turbulent spots, which from then onward populate very rapidly and eventually combine into turbulent flow, while retaining the counterrotating vortex character of the primary instability. This is the fourth and final stage. Eventually, turbulent diffusion evens out any spanwise velocity differences, resulting in near-homogeneous turbulence near the bend exit. The two preferred frequencies, 16 and 28 Hz, whose values are likely to be related to the specific characteristics of the present flow (disturbance source, curvature, flow rate, etc.) were attributed to the meandering motion and the horseshoe vortex movement, respectively. The normal distance y where the spectra indicated maximum energy in the preferred frequencies was consistent with the upwash high-shear zone, where the fluctuating velocities also peaked during transition [Figure 4(b)]. Figure 8 shows frequency spectra at upwash: (a) at $\varphi = 23°$, before transition, where only low frequencies appeared; (b) at $\varphi = 35°$, during transition, where the two preferred frequencies are seen together with higher frequency turbulence; and (c) at $\varphi = 54°$, after transition, where the preferred frequencies slowly fade out but the meandering motion still persists into the seemingly turbulent boundary layer. Spectra at downwash were similar, exhibiting a small lag, which suggests a rapid

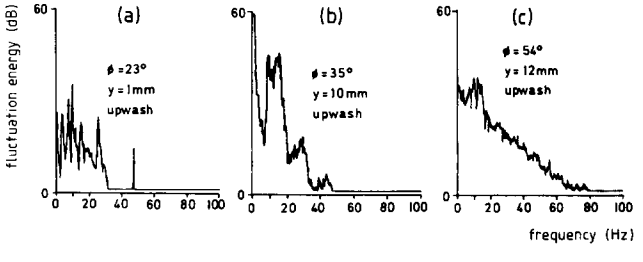

Figure 8 Representative energy spectra of unfiltered hot-film probe output

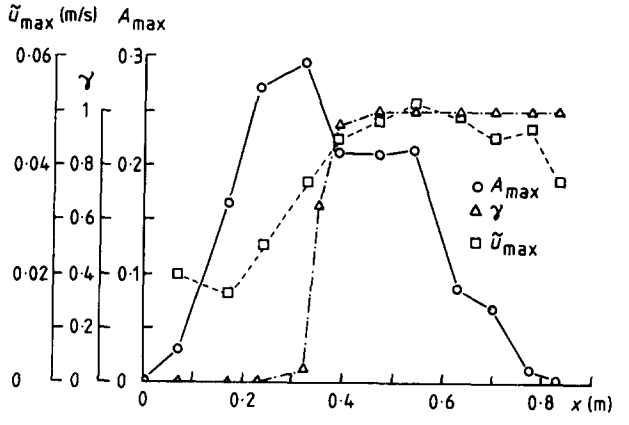

Figure 9 Streamwise variation of maximum (in y-direction) values of r.m.s. fluctuating velocity $\tilde{u}$, intermittency factor γ, and amplitude A of mean velocity distribution $\bar{u}(z)$ across span

lateral spread of turbulence, expected with the counterrotating motion redistributing momentum within the boundary layer.

The amplitude A of the spanwise distribution of $\bar{u}$ provided an indication of the state of the boundary layer. We define A as $\frac{1}{2}(\hat{\bar{u}}-\check{\bar{u}})_{max}/u_{pw}$, where $\hat{\bar{u}}$ and $\check{\bar{u}}$ are the mean velocity at downwash and upwash positions, respectively, and max denotes the maximum value as y is varied at a given x. As shown in Figure 9, A increased from 0 near bend entry to about 0.3 at transition start, and fell to 0.2 at transition end. The decrease in A following transition start was the result first of vortex unsteadiness and then of turbulent diffusion, which increasingly smeared out the time-mean spanwise variation in velocity. This variation in A, peaking at around 0.3, matches that found previously in another flow rig (see Ref. 24).

Consistency of the results with concave wall boundary layer stability theories[28] is demonstrated in Figure 10 by plotting the experimental results on a stability chart calculated by Finnis and Brown.[29] The values of G_θ plotted against $\alpha\theta$ (where α is the wave number $2\pi/\lambda$) lie on a straight line corresponding to constant wavelength $\lambda = 16$ mm (as measured).

A limited attempt was made to establish a criterion for transition start by varying the bulk flow velocity and detecting the location of transition start (defined by $\gamma = 10\%$). Over a range of Re_a from 6300 to 12,900, upwash Re_θ at transition start was between 460 and 500, which can be translated (using the model of Ref. 9) into approximately 400 for $\gamma = 0$–1%. This value is twice as high as predicted using published criteria as in Refs. 9 or 10 for the same free-stream turbulence level and zero pressure gradient on a flat surface. Furthermore, upwash Görtler numbers at transition start were in the region of 20–25; these are four to five times higher than predicted using Forest's[6] correlation, which uses a maximum limiting value of G_θ of 9. More extensive measurements, covering other vortex pairs of varying strength, would be necessary before attempts could be made to formulate any relationships for the concave wall equivalent to Equations 1–3.

Conclusions

After initial formation of the vortex structure in the early part of the bend, its development followed the well-documented linear and nonlinear stages before the onset of a meandering motion and a secondary horseshoe-type dynamic instability leading to transition. Transition appeared to start at the upwash region of a vortex pair—at a distance from the wall where the r.m.s. fluctuating velocity peaked in the high-shear layer.

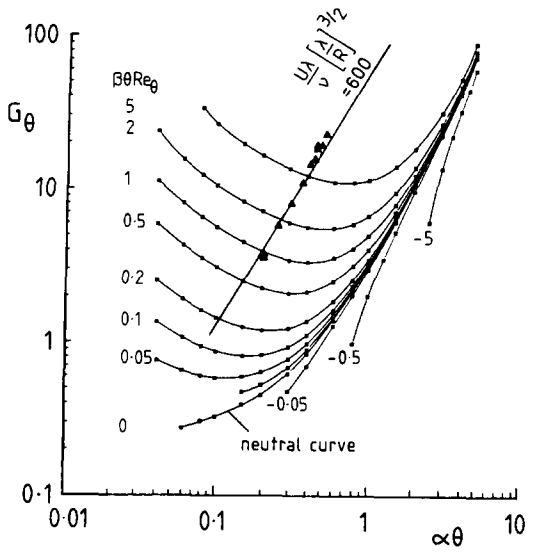

Figure 10 Görtler vortex stability diagram (from Ref. 29), showing present measurements (Δ, upwash–downwash averaged) at Re_a = 10,500 (α = wavenumber $2\pi/\lambda$, β = vortex amplification factor defined in Ref. 29)

Lateral spreading of turbulence to the downwash region was rapid. The transition region, as defined by a change in intermittency factor from 10% to about 90%, was short compared to those often inferred from heat transfer measurements on concave walls or blade cascade pressure surfaces; this result suggests that gradual rises in heat transfer above laminar levels may be caused in part by pretransitional vortex unsteadiness, a possibility highlighted by recent heat transfer measurements.[30] (In nominally 2-D blade boundary layers, a more straightforward explanation could be a fine balance between the opposing effects of high turbulence levels and strongly favorable pressure gradients.) The energy spectrum during flow breakdown on the concave wall showed two preferred frequencies, unlike those for flat plates.

Velocity profile distortion caused widely differing variations of Re_θ and G_θ between the upwash and downwash regions. Established correlations for start and length of transition on flat walls were found not to apply to the present flow. Upwash-localized and upwash–downwash averaged Re_θ at transition start were found to exceed those expected on a flat surface; this result is apparently at variance with the results of other investigations, but the present values are not representative of a spanwise average Re_θ as a result of vortex distortion after the linear phase of development. This result, together with previous work, suggests that Re_θ and G_θ are not necessarily appropriate parameters for formulating a transition criterion for concave walls. Other factors pointing toward this conclusion are the observations that vortex pairs at different stages of development coexist at the same streamwise location and also that integral boundary layer parameters (e.g., θ) are based on a dynamic layer development resulting not only from fluid viscosity but from effects related to the Görtler vortex presence as well.

Acknowledgment

G. Leoutsakos was supported by a Science and Engineering Research Council (SERC) Studentship. This work was partly funded by a SERC grant.

References

1 Daniels, L. C. and Browne, W. B. Calculation of heat transfer rates to gas turbine blades. *Int. J. Heat and Mass Transf.* 1980, **24**, 871

2 Rodi, W. and Scheuerer, G. Calculation of heat transfer to convection-cooled gas turbine blades. *J. Eng. Gas Turbines & Power* (Trans. ASME). 1985, **107**, 620

3 Han, L. S. and Cox, W. R. A visual study of turbine blade pressure-side boundary layers. *J. Eng. Power* (Trans. ASME). 1983, **105**, 47

4 Riley, S. Three-dimensional boundary layer transition. Ph.D. Thesis, University of Liverpool, 1986

5 Spalding, D. B. *GENMIX: A General Computer Program for Two-Dimensional Parabolic Phenomena*. Pergamon, Oxford, 1977

6 Forest, A. E. Engineering predictions of transitional boundary layers. AGARD-CP-224 Laminar-Turbulent Transition, 1977, 22-1

7 Wang, J. H., Jen, H. F., and Hartel, E. O. Airfoil heat transfer calculation using a low Reynolds number version of a two-equation turbulence model. *J. Eng. Gas Turbines & Power* (Trans. ASME). 1985, **107**, 60

8 Crane, R. I., Leoutsakos, G., and Sabzvari, J. Transition in pressure-surface boundary layers. *J. Turbomach.* (Trans. ASME). 1987, **109**, 296

9 Abu-Ghannam, B. J. and Shaw, R. Natural transition of boundary layers—the effects of turbulence, pressure gradient and flow history. *J. Mech. Eng. Sci.* 1980, **22**, 213

10 Seyb, N. A simplified and practical method of determining the external heat transfer coefficient round a turbine blade. Aeronautical Research Council Report ARC 29398, 1967

11 Dunham, J. Prediction of boundary layer transition on turbomachinery blades. AGARD AG-164, No. 3, 1972

12 Van Driest, E. R. and Blumer, C. B. Boundary layer transition: Free-stream turbulence and pressure gradient effects. *AIAA J.* 1968, **1**, 1303

13 Dhawan, S. and Narasimha, R. Some properties of boundary layer flow during the transition from laminar to turbulent motion. *J. Fluid Mech.* 1957, **3**, 418

14 Leoutsakos, G. Boundary layer transition on concave surfaces. Ph.D. Thesis, University of London, 1987

15 So, R. M. C., Edelfelt, I. H., Elovic, E. and Kercher, D. A two-dimensional boundary layer program for turbine airfoil heat transfer calculation. ASME Paper 82-GT-93, 1982

16 Liepmann, H. W. Investigation of laminar boundary layer stability and transition on curved boundaries. NACA Wartime Rept. ACR 3H30, 1943

17 Shigemi, M. and Gibbings, J. C. Boundary layer transition on a concave surface. Inst. Mech. Engrs. Paper No. C262/87, 1987

18 Bradshaw, P. Effects of streamline curvature on turbulent flow. AGARD AG-169, 1973

19 So, R. M. C. A turbulence velocity scale for curved shear flows. *J. Fluid Mech.* 1975, **70**, 37

20 Gibson, M. M. An algebraic stress and heat flux model for turbulent shear flow with streamline curvature. *Int. J. Heat and Mass Transf.* 1978, **21**, 1609

21 Jones, W. P. and Launder, B. E. The prediction of laminarisation with a two-equation model of turbulence. *Int. J. Heat and Mass Transf.* 1973, **16**, 1189

22 Brown, A. and Martin, B. W. Flow transition phenomena and heat transfer over the pressure surfaces of gas turbine blades. *J. Eng. Power* (Trans. ASME). 1982, **104**, 360

23 Gaugler, R. E. Some modifications to, and operational experience with, the two-dimensional finite-difference boundary layer code STAN5. ASME Paper 81-GT-89, 1981

24 Crane, R. I. and Sabzvari, J. Laser-Doppler measurements of Görtler vortices in laminar and low-Reynolds-number turbulent boundary layers. *Laser Anemometry in Fluid Mechanics*, ed. Adrian, R. J. *et al.* LADOAN-Inst. Tec. Sup., Lisbon, 1984

25 Bippes, H. and Görtler, H. Dreidimensionale Störungen in der Grenzchicht an einer Konkaven Wand. *Acta Mech.* 1972, **14**, 251

26 Aihara, Y. and Koyama, H. Secondary instability of Görtler vortices: Formation of a periodic three-dimensional coherent structure. *Trans. Japan Soc. Aero Space Sci.* 1981, **24** (Pt. 64), 78

27 Swearingen, J. D. and Blackwelder, R. F. The growth and breakdown of streamwise vortices in the presence of a wall. *J. Fluid Mech.* 1987, **182**, 255

28 Görtler, H. On the three-dimensional instability of laminar boundary layers on concave walls. NACA TM1375 (English transl.), 1954

29 Finnis, M. V. and Brown, A. Stability of a laminar boundary layer flowing along a concave surface. ASME Paper 88-GT-40, 1988

30 Crane, R. I. and Sabzvari, J. Heat transfer visualization and measurement in unstable concave-wall laminar boundary layers. *J. Turbomach.* (Trans. ASME). 1989, **111**, 51